# A Four-Quadrant Thrust Estimation Scheme for Marine Propellers: Theory and Experiments

Luca Pivano, Tor Arne Johansen and Øyvind N. Smogeli

***Abstract*— A thrust estimation scheme for marine propellers that can operate in the full four-quadrant range of the propeller shaft speed and the vessel speed has been developed. The scheme is formed by a nonlinear observer to estimate the propeller torque and the propeller shaft speed and by a mapping to compute the thrust from the observer estimates. The mapping includes the estimation of the propeller advance ratio. The advance speed is assumed to be unknown, and only measurements of shaft speed and motor torque have been used. The robustness of the scheme is demonstrated by Lyapunov theory. The proposed method is experimentally tested on an electrically driven fixed pitch propeller in open-water conditions, in waves and with a wake screen that scales the local flow down in order to simulate one of the effects of the interaction between the propeller and the vessel hull.**

***Index Terms*— estimation, nonlinear, marine propulsion.**

## I. Introduction

In marine guidance, navigation and control (GNC) systems, the low level thruster controllers have traditionally received less attention compared to the guidance system and the high-level plant control. In the design of Dynamic Positioning (DP), thruster assisted Position Mooring (PM) and autopilot systems, for example, much effort has been put into the high-level control schemes and the propeller dynamics has often been neglected. More recently, also the issue of thruster dynamics and control has received more attention. For recent references, see for example [1], [4], [8], [12], [20], [27], [29], [31], [32] and the references therein. The main difficulties in the design of effective propeller controllers lie in the modeling of the propeller's dynamics and in the problem of measuring the environmental state.

When a ship performs a marine operation, propellers are often affected by thrust losses due to cross flow, ventilation, in-and-out-of water effects, wave-induced water velocities, interaction between the vessel hull and the propeller and between propellers. Propellers may thus work far from ideal conditions therefore, knowledge of the propeller thrust and torque, together with the thrust induced pressure force on the hull, is fundamental to achieve high vessel control performance. The knowledge of the propeller thrust, either measured or estimated, could also allow the design of controllers for reducing power fluctuations and wear and tear in high sea state. Moreover, the performance monitoring is also useful for improving fault detection and thrust allocation in different propeller working conditions.

These considerations motivate the development of schemes to estimate the propeller thrust because, in general, its measurement is not available. The estimated value of the thrust could be used for underwater vehicles for example, in observers for the estimation of the ocean current [7] and in adaptive schemes for the identification of the vehicle hydrodynamic drag [24]. Recently, observers for monitoring the propeller performance have been developed and included in new control designs for electrically driven propellers, see [3], [10], [18], [21], [25], and [28].

The problem of propeller thrust estimation has been treated in [33], where full-scale experimental results were provided in steady-state conditions, in waves, and for inclined inflow. The estimation was based on the propeller torque measurement and on a linear relation between thrust and torque. Experimental results were presented only for positive shaft speed and vessel speed. Steady-state thrust estimates can also be obtained from thrust and torque identity techniques [6] which assume the knowledge of the propeller torque, used to compute an equivalent open water advance ratio. This is combined with open-water propeller characteristics, corrected for scale effects, to obtain the thrust estimate. Thrust estimation has been also treated in [10], where the estimate was computed from the propeller torque obtained with a Kalman filter where a linear shaft friction torque was considered. The relation between thrust and torque involved an axial flow velocity model and requires the knowledge of the advance speed. The scheme was also highly sensitive to hydrodynamic and mechanical modeling errors. The performance was validated by simulations.

An adaptive observer to estimate shaft speed and thrust was also designed for variable pitch propulsion systems in [3] and [18]. The observer was used for fault detection in the shaft speed control loop. A linear approximation of the propeller characteristics was utilized, therefore this approach could not guarantee accurate results in all four quadrant plane composed by the vessel speed and the propeller shaft speed. Moreover, the observer employed the vessel speed measurement.

The contribution of this paper is the development of a four-quadrant thrust estimation scheme, extending the preliminary results described in [22] and [23]. The strength of the presented approach is that only measurements of the propeller shaft speed and the motor torque, normally available on ships, are utilized. Differently from [10], the advance speed which is very difficult to measure in real vessels, is assumed to be unknown.

This work has been supperted by the Norwegian Research Council.

L. Pivano and T. A. Johansen are with Department of Engineering Cybernetics, Norwegian University of Science and Technology, NO-7491 Trondheim, Norway. E-mail: [luca.pivano,tor.arne.johansen]@itk.ntnu.no

Ø. N. Smogeli is with Marine Cybernetics, NO-7075 Tiller, Norway. E-mail: [Oyvind.Smogeli@marinecyb.com]

Our scheme is based on a robust nonlinear observer to estimate the propeller torque and the shaft speed, and on a mapping to compute the propeller thrust from the observer estimates. The observer is similar to the one introduced in [28], but the inclusion of a nonlinear friction term is a new contribution. Moreover, in order to analyze the effect of the measurement and friction modeling errors on the observer estimates, a Lyapunov based robustness analysis has been performed. The thrust is computed from the torque estimate through a mapping that involves the estimation of the advance ratio. The performance of the proposed scheme is demonstrated by extensive experiments carried out on an electrically driven fixed pitch propeller in a basin with close to open-water conditions, in waves and with a wake screen that scales the local flow down in order to simulate one of the effects of the interaction between the propeller and the vessel hull.

The paper is organized as follows. The overall propulsion system is described in Section II. The experimental setup and instrumentation are presented in Section III. Modeling of the propeller shaft dynamics, thrust and torque, and the open-water characteristics is treated in Section IV. The thrust estimation scheme is described in Section V and experimental results are presented in Section VI. Finally, the conclusions are given in Section VII.

## II. Overall System Description

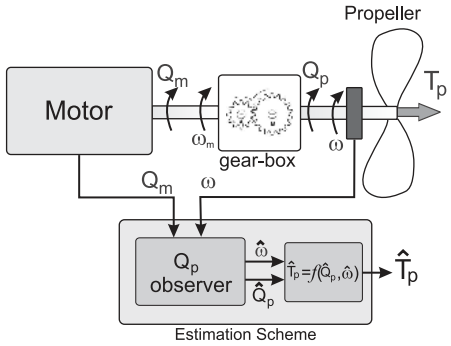


Fig. 1. Block diagram of the propeller system and the thrust estimation scheme.

A block diagram that represents the propeller system and the scheme implemented to estimate the propeller thrust is shown in Fig. 1. The propeller is connected to the motor through a shaft and a gear box. The motor torque applied to the shaft is denoted $Q_m$. The gear ratio is defined by $R_{gb} = \omega_m/\omega$, where $\omega_m$ is the motor shaft angular speed and $\omega$ is the propeller angular speed. The value of $\omega$ is particularly influenced by the load, represented by the propeller torque $Q_p$, due to the rotation of the blades in the water. The output of the system is the thrust $T_p$ produced by the propeller.

The thrust estimation scheme includes a nonlinear observer that computes the estimate $\hat{Q}_p$ of the propeller load torque and the estimate $\hat{\omega}$ of the shaft speed. The observer uses the measurements of the motor torque $Q_m$ and the propeller shaft speed $\omega$. An estimate $\hat{T}_p$ of the propeller thrust is computed using the observer estimates $\hat{Q}_p$ and $\hat{\omega}$ through a mapping $f$.

## III. Experimental Setup and Instrumentation

The tests were carried out at the Marine Cybernetics Laboratory, an experimental laboratory located at NTNU in Trondheim. The basin, 6.45 m wide, 40 m long and 1.5 m deep, is equipped with a 6DOF towing carriage that can reach a maximum speed of 2 m/s and with a wave generator able to generate waves up to 0.3 m. The tank dimensions may appear too small for accurate open-water and dynamic tests due to the influence of previous motions, presence of walls and free surface motion. The variance of the obtained results was found to be small. We employed a three phase brushless motor in combination with a drive equipped with a built-in torque controller and a build-in shaft speed controller. In this way we could choose to control the motor torque in order to obtain the desired motor torque or the shaft speed to obtain the desired $\omega$. The motor was connected to the propeller shaft through a gear-box with ratio 1:1. The rig with motor, underwater housing, shaft and propeller was attached to the towing carriage in order to move the propeller through the water. The tests were performed on a fixed pitch propeller without duct and with geometric parameters given in Table I. The real-time system Opal RT-Lab® was used to interface the Matlab/Simulink® environment to the motor drive and the sensors. The shaft speed was measured on the motor shaft with a tachometer dynamo. The thrust and torque were measured with an inductive transducer and a strain gauge transducer placed on the propeller shaft, respectively. The measurement of the motor torque was furnished by the motor drive. All the signals were acquired at the frequency of 200 Hz. A sketch of the setup is shown in Fig. 2 and a picture of the propeller system is presented in Fig. 3.

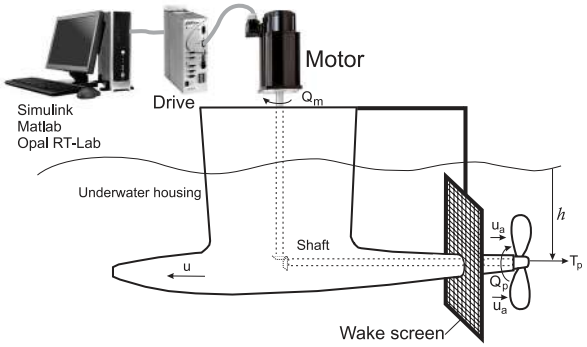


Fig. 2. Sketch of the experimental setup.

TABLE I
P1362 PROPELLER GEOMETRICAL PARAMETERS

| Parameter | Value | Description |
|---|---|---|
| $D$ | $0.25\ m$ | Propeller diameter |
| $Z$ | $4$ | Number of blades |
| $P/D$ | $1.0$ | Pitch ratio P/D |
| $A_e/A_0$ | $0.55$ | Expanded blade area ratio |

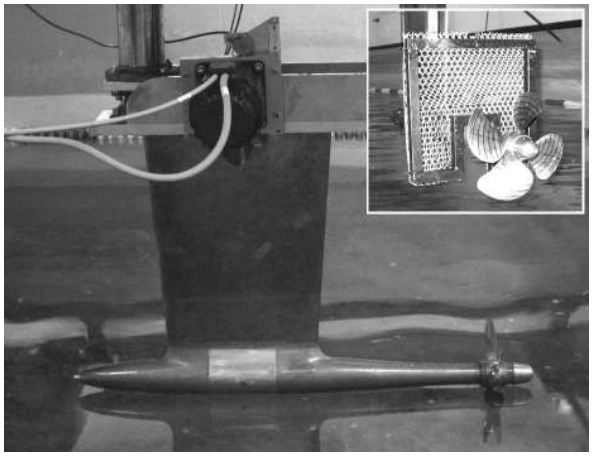

Fig. 3. Propeller open-water configuration (main picture) and wake screen (small picture).

## IV. Propeller Modeling

### A. Propeller shaft dynamics

The shaft dynamics is derived by considering the motor connected to the propeller through a rigid shaft and a gearbox with gear ratio $R_{gb}$, as shown in the block diagram of Fig. 1. The shaft is considered affected by a friction torque denoted $Q_f(\omega)$, which is assumed to depend only on the shaft speed. The shaft dynamics can be written as

$$J_m\dot{\omega} = R_{gb}Q_m - Q_p - Q_f(\omega), \tag{1}$$

where $J_m$ is total moment of inertia including the shaft, the gear box and the propeller. The friction torque has been modeled as

$$Q_f(\omega) = k_{f_1}\arctan\left(\frac{\omega}{\epsilon}\right) + k_{f_2}\omega + k_{f_3}\arctan(k_{f_4}\omega), \tag{2}$$

where the Coulomb effect, usually written as a $\mathrm{sign}(\omega)$, has been replaced by the function $\frac{2}{\pi}\arctan(\frac{\omega}{\epsilon})$ with a small positive $\epsilon$ in order to avoid the singularity for $\omega = 0$. The remaining terms in (2) represent a linear and a nonlinear viscous effect. All the coefficients $k_{f_i}$ are constant and positive. The static friction model (2) is able to approximate the friction torques experienced in practice (see [1], [16] and [22]).

*1) Shaft moment of inertia and friction torque identification:* To identify the friction torque and the shaft moment of inertia in (1), we ran tests with different motor torque profiles and various towing carriage speeds. From the measurement of the propeller angular speed, the motor torque and the propeller torque, and computing the derivative of $\omega$ with the necessary filtering, we identified the parameters $k_{f_i}$ of the friction torque model (2) and the shaft moment of inertia $J_m$. The parameters $k_{f_i}$ and $J_m$ can be grouped in the vector

$$\theta = \begin{bmatrix} k_{f_1} & k_{f_2} & k_{f_3} & k_{f_4} & J_m \end{bmatrix}^T. \tag{3}$$

With $R_{gb} = 1$ and defining $z = Q_m - Q_p$, $\theta$ is computed over a time-series of $N$ samples as

$$\theta = \arg\min \sum_{i=1}^{N} |z_i - Q_f(\omega_i) - J_m\dot{\omega}_i|^2. \tag{4}$$

where the subscript $i$ indicates the i-th sample (see for examples [9]). The parameters obtained are shown in Table II.

TABLE II
Friction model parameters and shaft moment of inertia.

| Parameter | Value | Parameter | Value |
|---|---|---|---|
| $J_m[kg\cdot m^2]$ | $6.07\cdot 10^{-3}$ | $k_{f_3}[kg\cdot m^2/s]$ | $6.61\cdot 10^{-3}$ |
| $k_{f_1}[kg\cdot m^2/s]$ | $3.97\cdot 10^{-1}$ | $k_{f_4}[-]$ | $8.94\cdot 10^{-2}$ |
| $k_{f_2}[kg\cdot m^2/s]$ | $9.28\cdot 10^{-3}$ | $\epsilon[-]$ | $1\cdot 10^{-3}$ |

Figure 4 shows the friction torque computed from measurements and the identified model. The friction exhibits a nonlinear behavior and is affected by the temperature in the gears, bearings and oil. The friction presents also a hysteresis effect but its influence is not very significant and it has been neglected.

For the tested propeller system, the losses due to the friction torque are quite high compared to a full scale propeller, where they are usually less significant.

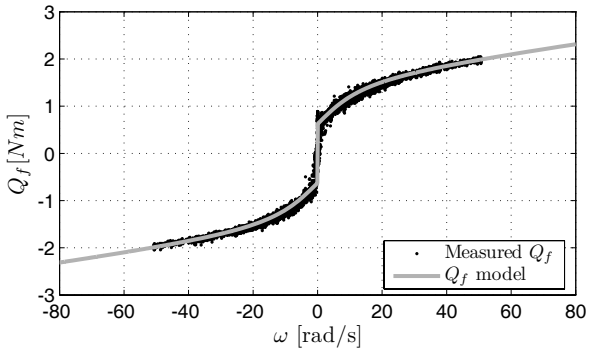


Fig. 4. Friction torque: computed from measurements and the identified nonlinear static model.

### B. Propeller thrust and torque

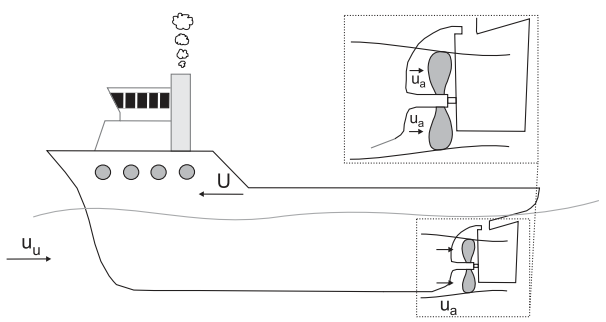


Fig. 5. Definition of the advance speed $u_a$ and vessel speed $U$ and the undisturbed flow speed $u_u$.

Modeling the thrust and torque produced by a propeller is a complicated task, since it is difficult to develop a finite-dimensional analytical model from the laws of physics. This is mainly due to the difficulty in modelling the flow dynamics, especially when the flow is not uniform [1], [4], [5], [12], [16], [20]. The thrust and torque depend also on the propeller geometric parameters (i.e. propeller diameter, pitch angle, etc.), the non-dimensional parameters advance ratio $J$ and Reynolds number, the propeller submergence and environmental state (waves, currents, etc.). A common practice is the use of simplified models which are chosen based on the propeller application. See for example [8], [21] and [28] and the references therein.

*1) Open-Water propeller characteristics:* Neglecting the effect of waves and marine currents, and assuming a deeply submerged fixed pitch propeller, the thrust and torque are usually represented in nondimensional form. One form is represented by the standard open-water coefficients $K_T$ and $K_Q$, given as functions of the advance ratio $J$. The term open-water refers to the case where the propeller is tested without the presence of a vessel hull. The coefficients $K_T$ and $K_Q$ are computed from [6] as

$$K_T = T_p \frac{4\pi^2}{\rho \left|\omega\right| \omega D^4}, \tag{5}$$

$$K_Q = Q_p \frac{4\pi^2}{\rho \left|\omega\right| \omega D^5}, \tag{6}$$

where $\rho$ is the density of the water and $D$ is the propeller diameter. The advance ratio is computed as

$$J = \frac{2\pi u_a}{\omega D}, \tag{7}$$

where $u_a$ is the advance speed, i.e. the water inflow velocity to the propeller. The $K_T$ and $K_Q$ curves are measured for a range of propeller advance numbers $J$, usually in a cavitation tunnel or a towing tank [14]. When the propeller is working in water that has been disturbed by the passage of the hull, it is no longer advancing relatively to the water at the speed of the ship $U$, but at some different speed $u_a$. The advance speed is very difficult to measure and an estimate of $u_a$ is usually computed using the steady-state relation

$$u_a = (1 - w)U, \tag{8}$$

where $w$ is the *wake fraction number,* often identified from experimental tests (see e.g. [17]). Figure 5 shows a sketch of a vessel with the velocities involved. The surge vessel speed $U$ is relative to the earth while $u_a$ is the longitudinal water speed relative to the propeller disc. The undisturbed water velocity $u_u$ has the same magnitude as the vessel speed but with opposite direction.

A measure of the propeller performance is the open-water efficiency, which is defined as the ratio of the produced to the consumed power by the propeller. The propeller efficiency is usually plotted for positive values of $J$ and is computed from (5), (6) and (7) as

$$\eta = \frac{u_a T_p}{\omega Q_p} = \frac{u_a K_T}{\omega D K_Q} = \frac{J K_T}{2\pi K_Q}. \tag{9}$$

The curves $K_T$ and $K_Q$ are usually employed in the first and in the third quadrant of the plane composed by $u_a$ and $\omega$, and they are not defined for $\omega = 0$. For propellers operating in the whole plane ($u_a$,$\omega$), four-quadrant open-water characteristics are normally utilized [6]. The four-quadrant coefficients $C_T$ and $C_Q$ are plotted as functions of the advance angle $\beta$. The value of $\beta$ is computed with the four quadrant inverse tangent function as

$$\beta = \arctan2\left(u_a, 0.7R\omega\right), \tag{10}$$

where $R$ is the propeller disc radius. The four-quadrant coefficients are calculated from [6] as

$$C_T = \frac{T_p}{\frac{1}{2}\rho V_r^2 A_0}, \tag{11}$$

$$C_Q = \frac{Q_p}{\frac{1}{2}\rho V_r^2 A_0 D}, \tag{12}$$

where $A_0$ is the propeller disc area and $V_r$ is the relative advance velocity:

$$V_r^2 = u_a^2 + (0.7R\omega)^2. \tag{13}$$

*2) Measured open-water characteristics:* To measure the open-water propeller characteristics, we performed tests at different values of the advance ratio $J$. To obtain the desired shaft speed $\omega$, the built-in speed controller of the drive was used. In our setup, the housing that contains gear and measurement devices does not create a significant wake and the advance speed $u_a$ has been considered equal to the towing carriage speed $U$. This yields a wake fraction number $w$ equal to zero. The standard propeller characteristics are plotted in Fig. 6. In Fig. 7 a sample of filtered data used to derive the $K_T$ and $K_Q$ curves are plotted. For positive $u_a$ and $\omega$, the inflow to the propeller is uniform and the thrust and torque are quite steady. When the advance speed becomes negative, the propeller tries to reverse the inlet flow and a recirculation zone (often called a ring vortex) occurs [30]. This is due to the interaction between the inlet flow and the reversed flow. The flow then becomes unsteady and can cause oscillations in the propeller thrust and torque. For negative values of $J$, $K_T$ and $K_Q$ were computed from the average of the measured thrust and torque.

From Fig. 6, it can be noticed that the tested propeller is not symmetric in the thrust production with respect to the shaft speed. For positive values of $\omega$ the efficiency is higher because the propeller was designed to work mainly at forward vessel speed.

Figure 8 shows the four-quadrant propeller characteristics and an approximation computed with a 25$^{\text{th}}$ order Fourier series, commonly adopted for the $C_T$ and $C_Q$ curves [6] .

*3) Torque model for the observer:* In order to estimate the propeller torque with an observer, a dynamic model for $Q_p$ is developed. The propeller torque $Q_p$ is treated as a time-varying parameter and modeled as a first order process with a positive time constant $\tau_1$, driven by a bounded noise $w_1$ as in [22], [23] and [26]:

$$\dot{Q}_p = -\frac{1}{\tau_1} Q_p + w_1. \tag{14}$$

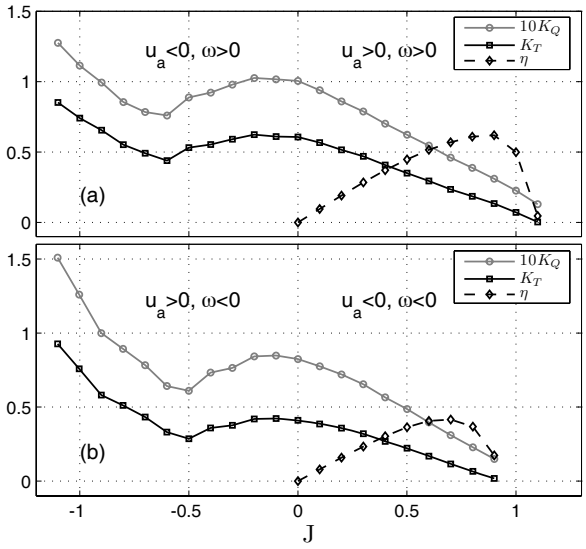


Fig. 6. Measured standard propeller characteristics: positive $\omega$ (a) and negative $\omega$ (b).

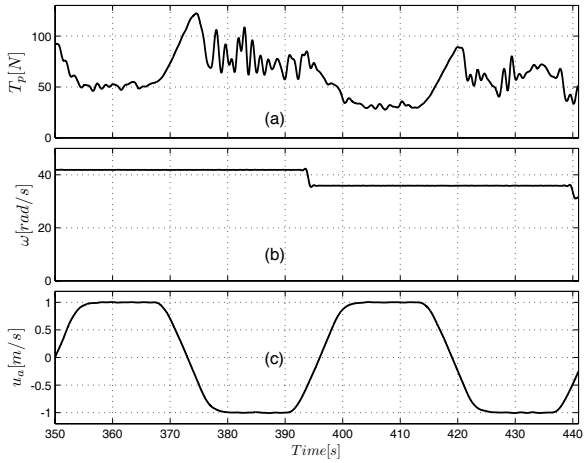


Fig. 7. Sample of measured data used to compute the propeller characteristics.

The proposed model does not have a structure related to the propeller hydrodynamics and geometry, but it is often used for the estimation of unknown variables. This is motivated by the fact that precise models often involve variables which are not measured or are known with large uncertainty, like flow velocities. In [1] and [20] more accurate dynamic models of thrust and torque have been developed. Both models use measurements of the advance speed and the axial flow velocity, the speed of the water at the propeller disc, which are difficult to measure on a real vessel.

## V. Thrust Estimation Scheme

This section presents the thrust estimation scheme. The required accuracy for the thrust estimate usually depends upon the application. For example, for ships that perform DP operations and low speed maneuvering, it is important to obtain accurate estimates in all quadrants since they may be equally explored, in certain sea and weather conditions.

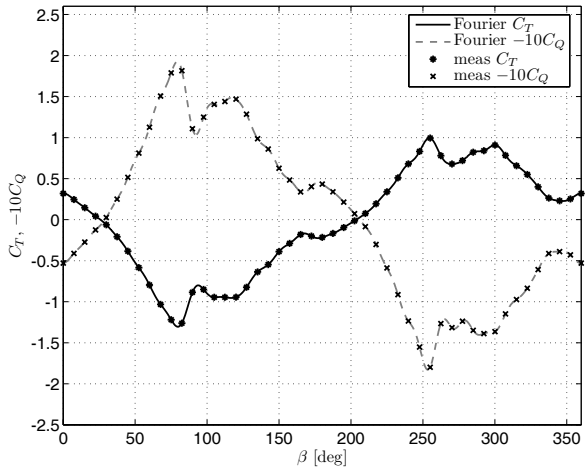


Fig. 8. Measured propeller four-quadrant open-water characteristics.

For ship in transit, however, only the first quadrant is usually explored therefore the accuracy required in the other quadrants is not particularly high.

### A. Propeller torque observer

The observer is based on the shaft dynamics and on the torque model described in the previous section. The motor torque $Q_m$ and the shaft speed $\omega$ are assumed to be measurable. For electric motors, the motor torque can be computed quite accurately from the motor current. For diesel engines, the motor torque can be measured with strain gauges on the motor shaft [2] or by measuring the fuel index [3].

From the shaft dynamics (1), the friction model (2) and the propeller torque (14), adding the measurement and modeling errors, the overall propeller dynamics can be written as

$$\begin{aligned} J_m\dot{\omega} = \quad & R_{gb}Q_m - Q_p + \Delta_f - k_{f_1}\arctan\left(\tfrac{\omega}{\epsilon}\right) - k_{f_2}\omega \\ & -k_{f_3}\arctan(k_{f_4}\omega), \\ \dot{Q}_p = \quad & -\tfrac{1}{\tau_1}Q_p + w_1. \end{aligned} \tag{15}$$

The output of the system is represented by

$$y = \omega + v, \tag{16}$$

where $v$ is a bounded measurement error. A friction torque modeling error and the measurement error on $Q_m$ are accounted for by $\Delta_f$, assumed to be bounded. Defining with $\hat{y} = \hat{\omega}$ the estimate of the angular shaft speed and with $\hat{Q}_p$ the estimate of the propeller torque, the following observer with gains $l_1$ and $l_2$ is proposed:

$$\begin{aligned} J_m\dot{\hat{\omega}} = \quad & R_{gb}Q_m - \hat{Q}_p - k_{f_1}\arctan(\tfrac{\hat{\omega}}{\epsilon}) - k_{f_2}\hat{\omega} \\ & -k_{f_3}\arctan(k_{f_4}\hat{\omega}) + l_1(y-\hat{y}), \\ \dot{\hat{Q}}_p = \quad & -\tfrac{1}{\tau_1}\hat{Q}_p - l_2(y-\hat{y}). \end{aligned} \tag{17}$$

The noise and errors can be treated as inputs, grouped in the vector $u$:

$$u \quad = [u_1 \quad u_2 \quad u_3]^T = [\Delta_f \quad v \quad w_1]^T. \tag{18}$$

With $\tilde{e}_1 = \omega - \hat{\omega}$ and $\tilde{e}_2 = Q_p - \hat{Q}_p$, the observer error dynamics can be written as:

$$\begin{array}{rl} \dot{\tilde{e}}_1 = & \frac{1}{J_m}\left[-\tilde{e}_2 - k_{f_1}\left(\arctan\left(\frac{\omega}{\epsilon}\right) - \arctan\left(\frac{\hat{\omega}}{\epsilon}\right)\right)\right] \\ & -\frac{k_{f_3}}{J_m}\left[\arctan\left(k_{f_4}\omega\right) - \arctan\left(k_{f_4}\hat{\omega}\right)\right] \\ & +\frac{1}{J_m}\left[-k_{f_2}\tilde{e}_1 - l_1\tilde{e}_1 + u_1 - l_1 u_2\right] \\ \dot{\tilde{e}}_2 = & -\frac{1}{\tau_1}\tilde{e}_2 + l_2\tilde{e}_1 + l_2 u_2 + u_3. \end{array} \tag{19}$$

Substituting $\omega = \tilde{e}_1 + \hat{\omega}$ in (19), we can group the nonlinearities in the following function:

$$\begin{array}{rl} \psi(\tilde{e}_1, \hat{\omega}) = & +\frac{k_{f_1}}{J_m}\left(\arctan\left(\frac{\tilde{e}_1+\hat{\omega}}{\epsilon}\right) - \arctan\left(\frac{\hat{\omega}}{\epsilon}\right)\right) \\ & +\frac{k_{f_3}}{J_m}\left(\arctan\left(k_{f_4}\left(\tilde{e}_1 + \hat{\omega}\right)\right) - \arctan\left(k_{f_4}\hat{\omega}\right)\right), \end{array} \tag{20}$$

where $\psi(\tilde{e}_1, \hat{\omega})$ has the property that $\forall \tilde{e}_1, \forall \hat{\omega}$, $\tilde{e}_1\psi(\tilde{e}_1, \hat{\omega}) \geq 0$. With $\tilde{e} = [\tilde{e}_1 \;\; \tilde{e}_2]^T$ and using (20), we can rewrite the observer error dynamics (19) as

$$\dot{\tilde{e}} = \quad -A_1\tilde{e} - F_1(\tilde{e}_1, \hat{\omega}) + B_1 u \quad , \tag{21}$$

where

$$A_1 = \begin{bmatrix} \frac{1}{J_m}\left(k_{f_2} + l_1\right) & \frac{1}{J_m} \\ -l_2 & \frac{1}{\tau_1} \end{bmatrix}, \tag{22}$$

$$F_1(\tilde{e}_1, \hat{\omega}) = \begin{bmatrix} \psi(\tilde{e}_1, \hat{\omega}) \\ 0 \end{bmatrix}, \tag{23}$$

$$B_1 = \begin{bmatrix} \frac{1}{J_m} & -\frac{l_1}{J_m} & 0 \\ 0 & l_2 & 1 \end{bmatrix}. \tag{24}$$

*Proposition 1:* If the parameters $\alpha, \mu$, $k$, and the observer gains $l_1$, $l_2$ are chosen such that

**A1** $\alpha > 0$ such that $\forall \tilde{e}_1$, $\forall \hat{\omega}$: $|\psi(\tilde{e}_1, \hat{\omega})| \leq \alpha\,|\tilde{e}_1|$,
**A2** $0 < \mu < \frac{2}{J_m}$,
**A3** $\kappa > 0$,
**A4** $0 < l_2 < \alpha^4\kappa^2 J_m$,
**A5** $l_1 > -k_{f_2} + \frac{l_2}{\alpha^2\kappa} + \frac{1}{2\mu\kappa}$,
then the system (19) is input-to-state stable (ISS).

*Proof:* See Appendix. ■

*Remark 2:* For the observer considered, there always exist parameter and gain values that can be chosen according to the above criteria.

The ISS property of the observer error dynamics provides the robustness of the observer against noise and modeling errors. The observer errors, and thus the torque and shaft speed estimates, remain bounded for any initial conditions regardless of the values of the measurement errors, the noise $w_1$ in the propeller torque model and the difference between the friction torque model and the actual friction. In particular, the observer robustness against friction torque modeling errors is very important. The shaft friction torque may depend upon variables which are not directly accounted for in the model, like temperature and bearing lubrication.

### *B. Thrust and torque relationship*

As stated above it is difficult to derive accurate models for the thrust and torque, especially when the inflow to the propeller is not uniform. For example, [1], [11] and [20] experimentally demonstrated the need of including the dynamics of the axial flow velocity at the propeller disc to obtain accurate thrust and torque models. Moreover, in [1] and [11] the modeling involved lift theory, and the thrust and torque were computed as functions of the lift and drag produced by the propeller blades. It is clear that thrust and torque are produced by the same physical phenomenon and are closely related. It is not wrong to think that in the value of propeller torque, some variables that influence the behavior of the propeller, like the axial flow velocity, for example, are implicitly hidden within. For this reason, it is possible to compute an estimate of the propeller thrust from the propeller torque and the shaft speed.

In this section a mapping to compute the propeller thrust from the torque that utilizes the standard propeller characteristics is presented. Even though the propeller characteristics are measured in steady-state conditions, we are able to achieve quite accurate results in all four-quadrants due to the close relationship between thrust and torque.

Considering the standard propeller characteristics and taking the ratio of (5) and (6), the steady-state propeller thrust can be expressed as

$$T_p = Q_p G_{QT}(J), \tag{25}$$

where

$$G_{QT}(J) = \frac{K_T}{K_Q D}, \tag{26}$$

is defined as the steady-state gain from the propeller torque to the thrust. This gain depends on the propeller working conditions and can be expressed as a function of the advance ratio $J$.

Since the advance speed is not measured, the value of $J$ is estimated in order to compute the value of $G_{QT}(J)$. A propeller does not usually work at values of $J$ greater than $1-1.2$ (depending on the propeller), where the produced thrust is negative, and for $J$ smaller than $-1.5$. Based on this, we limit our analysis to values of $J$ in the range $[-1.5, 1.1]$. However, when the shaft speed is reversed, the propeller works for a short time outside the range of $J$ that has been considered. In this condition, both thrust and torque are small since the shaft speed is small, and the approximation error of $G_{QT}(J)$ does not affect the estimation significantly. This is shown in the experimental results reported in Section VI.

The estimation of $J$ is performed using the estimates $\hat{Q}_p$ and $\hat{\omega}$. From (6), we can compute $\hat{K}_Q$, an estimate of $K_Q$ as

$$\hat{K}_Q = \hat{Q}_p \frac{4\pi^2}{\rho\hat{\omega}^2 D^5}, \quad \hat{\omega} \neq 0. \tag{27}$$

The value of $\hat{K}_Q$ has been limited by the upper bound $K_Q(J_{\min})$ and lower bound $K_Q(J_{\max})$ where $[J_{\min}, J_{\max}]$ is the range of $J$. In this way we handle also the case when $\hat{\omega} = 0$. An estimate $\hat{J}$ of the advance ratio can be derived by inverting the $K_Q$ curve and using the value of $\hat{K}_Q$ computed with (27). It can be noticed in part (a) of Figures 9 and 10, that the $K_Q$ curve is not invertible in the whole range of $J$ considered. For this reason, the $J$ axis has been divided in three zones. In zones 1 and 3 the $K_Q$ curve is invertible and an accurate estimate of $J$ can be computed. In zone 2, $\hat{J}$ has been approximated with zero to ensure correct thrust

estimation when the advance speed is zero, i.e. the vessel is at rest and not subjected to current. This approximation introduces an error on the estimate which is computed as

$$\hat{T}_p = \begin{cases} \hat{Q}_p G_{QT}(\hat{J})|_{\hat{\omega}\geq 0} & \hat{\omega} \geq 0 \\ \hat{Q}_p G_{QT}(\hat{J})|_{\hat{\omega}<0} & \hat{\omega} < 0. \end{cases} \quad (28)$$

Plots of the gains $G_{QT}(J)$ and $G_{QT}(\hat{J})$, for positive and negative values of $\omega$, are shown Figures 9 and 10. If $\hat{Q}_p$ and $\hat{\omega}$ are accurate, outside zone 2, $G_{QT}(\hat{J})$ approximates accurately $G_{QT}(J)$ and the estimated thrust is precise. In zone 2, $G_{QT}(\hat{J})$ is equal to $G_{QT}(0)$ and, due to the propeller characteristics, the difference between $G_{QT}(\hat{J})$ and $G_{QT}(J)$ is not of significant magnitude. In the border of zone 2, $G_{QT}(\hat{J})$ has been joined smoothly to $G_{QT}(0)$ in order to avoid sharp variation on the thrust estimate. For the tested propeller, the value of $J$ is limited to the range [-1.5,1.1] for $\omega \geq 0$ and to the range [-1.5,0.9] for $\omega < 0$. The maximum relative error between $G_{QT}(\hat{J})$ and $G_{QT}(J)$ is about 8% for $\omega \geq 0$ and 13% for $\omega < 0$.

A block diagram that represents the thrust estimation procedure is shown in Fig. 11.

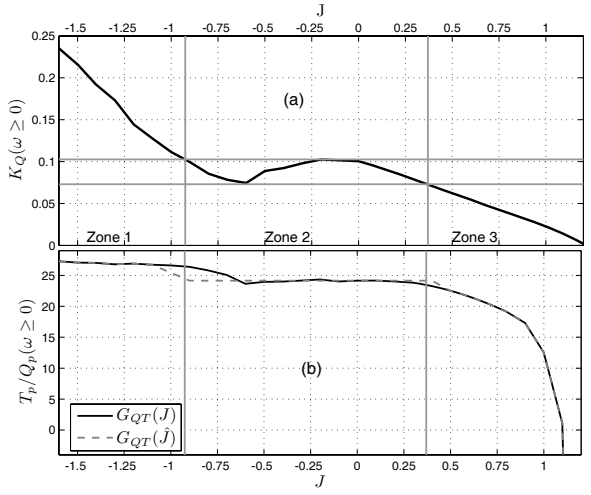


Fig. 9. Part (a): $K_q$ characteristic for positive $\omega$. Part (b): the ratio $G_{QT}(J)$ between thrust and torque computed from the propeller characteristics and its approximation $G_{QT}(\hat{J})$ for positive $\omega$.

*Remark 3:* On full scale vessels, the open-water characteristics obtained in a model scale is expected to be corrected for scale effects [13].

*Remark 4:* If the propeller open-water characteristics are not available, Computational Fluid Dynamics (CFD) techniques can help to derive it from the 3D drawing of the propeller, see for example [19] and references therein.

*Remark 5:* The thrust and torque relationship is not derived from the four-quadrant propeller characteristics because it is not possible to estimate the advance angle $\beta$ only from $\hat{Q}_p$ and $\hat{\omega}$, since we cannot compute the coefficient $C_Q$ without knowing $u_a$. This makes this parameterization difficult to use while we can estimate $J$ from $K_Q$, computed using $\hat{\omega}$ and $\hat{Q}_p$.

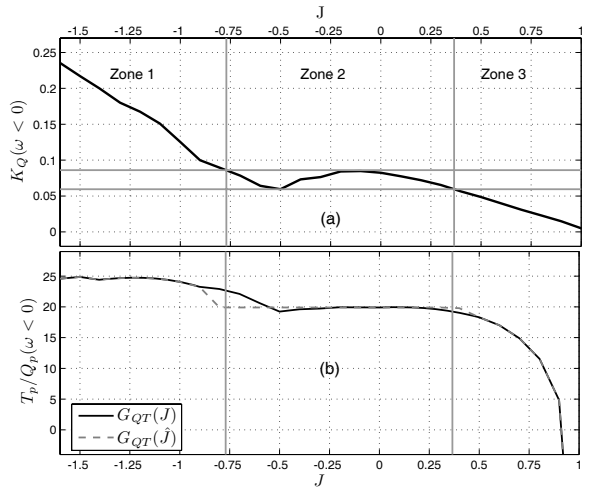


Fig. 10. Part (a): $K_q$ characteristic for negative $\omega$. Part (b): the ratio $G_{QT}(J)$ between thrust and torque computed from the propeller characteristics and its approximation $G_{QT}(\hat{J})$ for negative $\omega$.

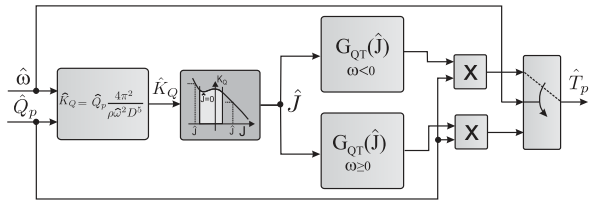


Fig. 11. Block diagram of the procedure to compute the propeller thrust from the estimated torque and shaft speed.

## VI. Experimental Results

### A. Observer tuning

The gains $l_1$, $l_2$ and the time constant $\tau_1$ for the torque observer in (17) were chosen as follows. The condition A1 of proposition 1 in Section V is satisfied with $\alpha = 1.7 \cdot 10^5$. This value is quite large due to the arctan function that represents the Coulomb friction, which presents a steep slope for values of $\omega$ close to zero. The conditions A2-A5 are satisfied with $\mu = 1$, $\kappa = 10$, and with

$$l_1 > 4.1 \cdot 10^{-2} + 3.5 \cdot 10^{-12} l_2,$$
$$0 < l_2 < 5 \cdot 10^{20},$$

which practically allows us to choose $l_1$ and $l_2$ freely. Considering the fact that we want the observer dynamics faster than the system dynamics and at the same time, too high gains can produce oscillatory estimates due to the measurement noise on the shaft speed, $l_1$ and $l_2$ were chosen as a trade-off between the two opposite requirements.

The time constant was obtained from a sensitivity analysis on the observer estimation errors with respect to $\tau_1$. Running the observer with $l_1 = 3\ kg \cdot m^2/s$, $l_2 = 80\ kg \cdot m^2/s^2$, on data acquired over more than 1 h of tests carried out in open-water conditions at different advance speeds and shaft speeds, we derived Fig. 12. The graph shows the root mean square error (RMSE) between the observer estimates and the

measurements. The value of the time constant has been varied between $0.01$ and $100$. For $\tau_1 \geq 1$, the accuracy of the estimates is practically the same, while for smaller values the estimate are less precise. For small values of $\tau_1$, the torque estimation error decreases when the shaft speed estimation error diminishes. This allows us to choose the time constant based on the speed error, since the torque measurements is not available in real cases. The observer parameters used in the experiments are $l_1 = 3\ kg \cdot m^2/s$, $l_2 = 80\ kg \cdot m^2/s^2$ and $\tau_1 = 10$ s.

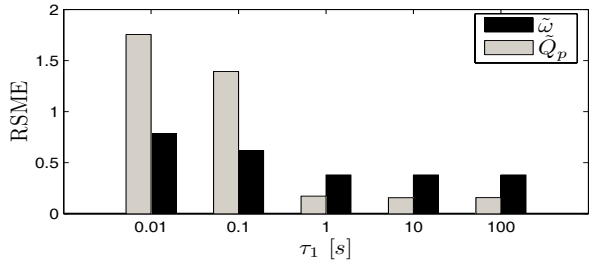


Fig. 12. Observer estimation errors for different values of $\tau_1$.

### B. Open water tests

A series of tests to validate the proposed scheme have been carried out in open-water conditions. The propeller was submerged at $h/R = 4$, where $h$ is the propeller submergence, in order to avoid losses due to ventilation. Figures 13 and 14 show data from an experiment where both the advance speed and the shaft speed had a trapezoidal form. Figures 15 and 16 show data from a test with sinusoidal advance and shaft speed.

The shaft speed and propeller torque estimates are plotted in part (a) and (c) of Figures 13 and 15, respectively. Both estimates are accurate and almost indistinguishable from the measurements. The observer estimation errors are plotted in part (b) and (d) of Figures 13 and 15. The advance speed is plotted in part (e) of the same figures.

Figures 14 and 16 show the measured and estimated thrust from the same tests. The estimated $\hat{T}_p$, shown in part (a), obtained with the proposed method reproduces quite well the measurements in all the quadrants. Part (e) of the same figures shows the advance angle $\beta$. The estimate $\hat{T}_p$ is compared with the estimate $\hat{T}_{p_{C_T}}$, shown in part (c), computed using the measured four-quadrant propeller characteristics $C_T$, introduced in Section IV, with $u_a = U$. This estimate is not very accurate, especially in the 2nd and 4th quadrant where the inflow to the propeller can be irregular. The proposed scheme furnish a more accurate thrust estimate since it can sense the effect of the flow variation through the propeller torque estimate. The thrust estimation errors are shown in (b) and (d) of Figures 14 and 16.

### C. Wake screen test

Tests with a wake screen, shown in Fig. 3, were performed to simulate one of the effects of the hull on the propeller inflow. The wake screen created an uniform loss of speed. This does not represent entirely the effect of the hull because the propeller inflow is not usually uniform. The propeller was submerged at $h/R = 4$.

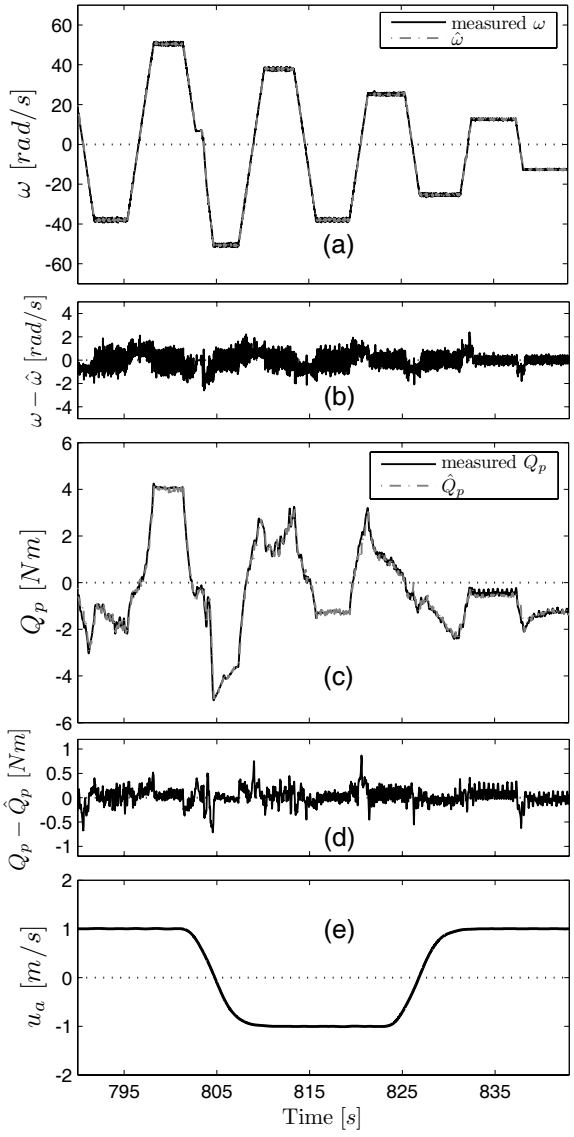


Fig. 13. Data from the first open-water test.

Figure 17 shows the results from a test where both the advance speed and the shaft speed had a trapezoidal form. As for the open-water experiments, the estimates provided by the observer, shown in (a) and (b), are very accurate. In (d) and (e) of the same plot, the estimate $\hat{T}_p$ obtained with the proposed method is compared with the estimate $\hat{T}_{p_{C_T}}$, computed using the measured four-quadrant propeller characteristic $C_T$. The advance speed is computed with (8), where the value of the wake fraction $w$ has been identified from tests performed in steady-state conditions. For positive towing carriage speed $U$, shown in (c), the experimentally found value was $w = 0.3$. For negative towing carriage speed, the inlet water flow to the propeller was not affected by the grid, placed upstream of the propeller, and the wake fraction number was zero. The estimate $\hat{T}_p$ is quite accurate also in this experiment while the estimate $\hat{T}_{p_{C_T}}$, as for the open-water tests, is accurate only

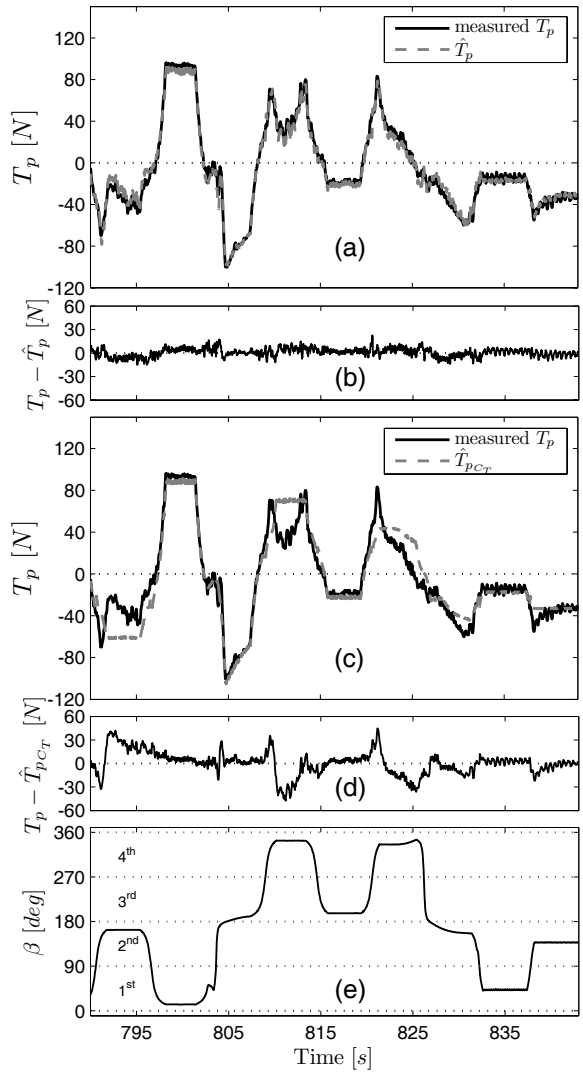


Fig. 14. Data from the first open-water test.

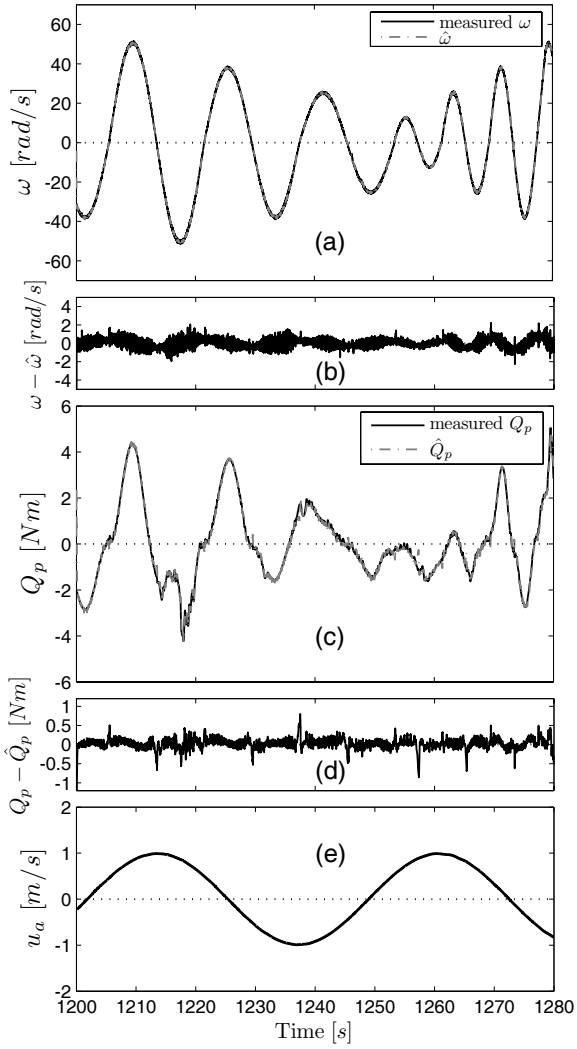


Fig. 15. Data from the second open-water test.

when $\omega$ and the $u_a$ have the same sign.

### D. Test in waves

Tests in waves were carried-out in order to validate the estimation scheme with a periodic propeller inflow and with large losses due to ventilation. Figure 18 shows the result of a test performed in regular waves with amplitude 0.05 m (equivalent to 0.2 $D$) and frequency 0.69 Hz. The propeller was also moved along its vertical axis with a sinusoidal motion. This was done to simulate the motion that a propeller may experience in rough sea conditions. This test does not reproduce entirely rough sea conditions but it may be a valid indication of the performance of the proposed method when operating in off-design conditions. The towing carriage was kept at rest ($U = 0$), but the advance speed was still not zero since the waves create an inflow to the propeller. Part (c) of Fig. 18 shows the propeller vertical displacement $d$. The propeller shaft speed, depicted in part (a), has been kept constant at 38 rad/s. A drop of thrust and torque occurred when the propeller rotated close to the water surface, since the load decreased due to ventilation. The small oscillations of thrust and torque were due to waves that created a periodic additional axial velocity component that varied with depth and time across the propeller plane. Both phenomena were well reproduced by the torque estimate, as shown in part (b) of Fig. 18. The thrust estimate $\hat{T}_p$ obtained from the proposed method is depicted in Fig. 18 (d) and is compared with $\hat{T}_{p_{C_T}}$, the thrust computed directly from the $C_T$ characteristic. The proposed method produced a satisfactory estimate and both the oscillations and the drop of thrust were properly captured. The estimate $\hat{T}_{p_{C_T}}$ has been computed assuming $u_a = 0$, the best guess we could make since $U = 0$. Since $\omega$ was constant and $u_a = 0$, the estimate $\hat{T}_{p_{C_T}}$ was constant and could not capture the thrust variations due to waves.

## VII. Conclusion

A thrust estimation scheme for a marine propeller has been developed and experimentally tested on an electrically driven propeller. Tests were performed in open-water conditions, with a wake screen to simulate one of the effects of the hull on the propeller inflow and in waves with vertical propeller motion in

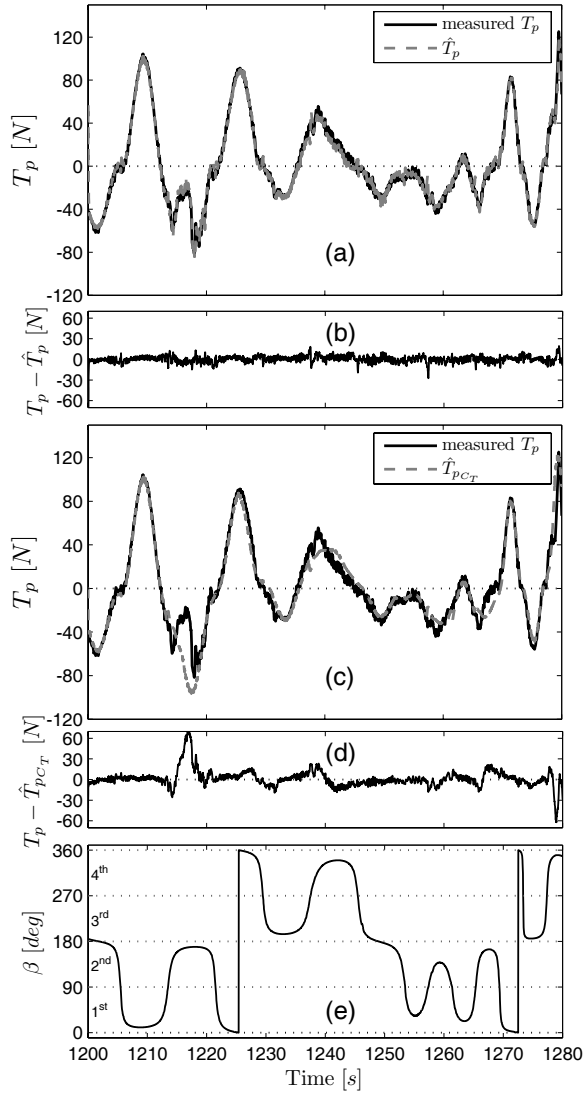


Fig. 16. Data from the second open-water test.

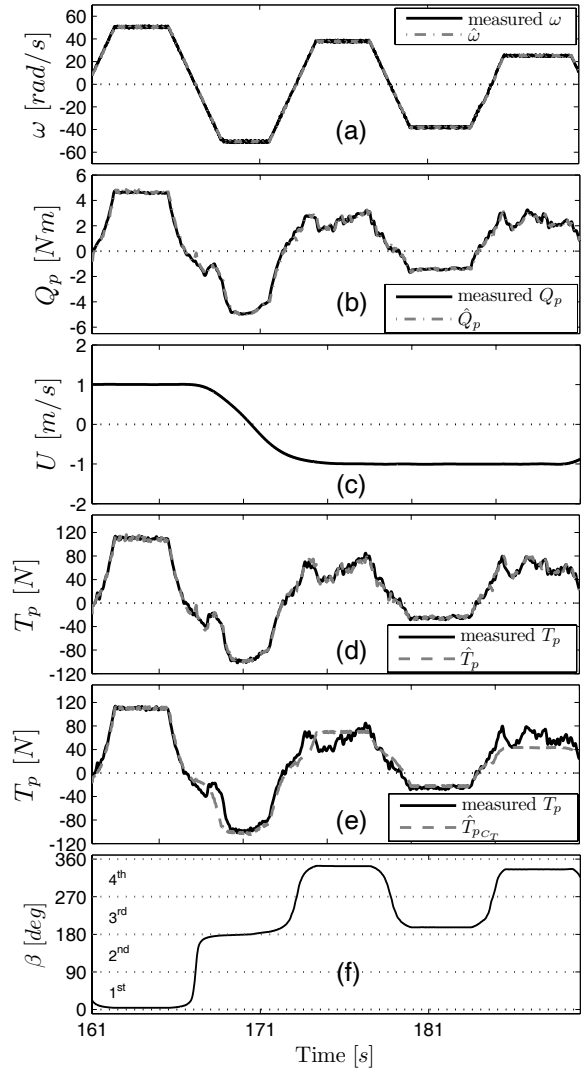


Fig. 17. Data from the wake screen experiment.

order to reproduce the motion that a propeller may experience in rough sea conditions. The robustness of the scheme with respect to modeling and measurement errors was demonstrated with the use of Lyapunov theory and corroborated by experimental results. The scheme involved a nonlinear observer to estimate the propeller torque and the shaft speed using only the measurements of the motor torque and the propeller shaft speed. The thrust estimate was computed from the estimated propeller torque and shaft speed involving the estimation of the advance ratio $J$. This only required knowledge of the standard propeller characteristics. The thrust obtained from the proposed method was compared with the thrust computed from the four-quadrant propeller characteristics showing improved accuracy in the estimates.

The thrust estimation scheme can be implemented also for ducted propellers, where the standard propeller characteristics are slightly different compared to a propeller without a duct.

Although the presented results concern tests carried out on an electrically driven propeller, the scheme could be applied also to propellers driven by diesel motors where the motor torque can be measured with strain gauges on the motor shaft [2] or by measuring the fuel index [3].

The presented results are promising for the use of such a thrust estimation scheme in high performance propeller controllers.

## VIII. Acknowledgments

The authors acknowledge with gratitude Professor Thor Inge Fossen for valuable suggestions and discussions. Matthias Schellhase is gratefully acknowledged for the help given during the experimental tests. The Research Council of Norway is acknowledged as the main sponsor of this project.

## Appendix

The appendix presents the proof of Proposition 1.

First we consider the input $u$, defined in (18), equal to zero $\forall t$ and later we investigate its effect on the error dynamics. Taking the Lyapunov function candidate $V := \frac{1}{2}\tilde{e}^T P_1 \tilde{e}$, where $P_1 = P_1^T > 0$ and

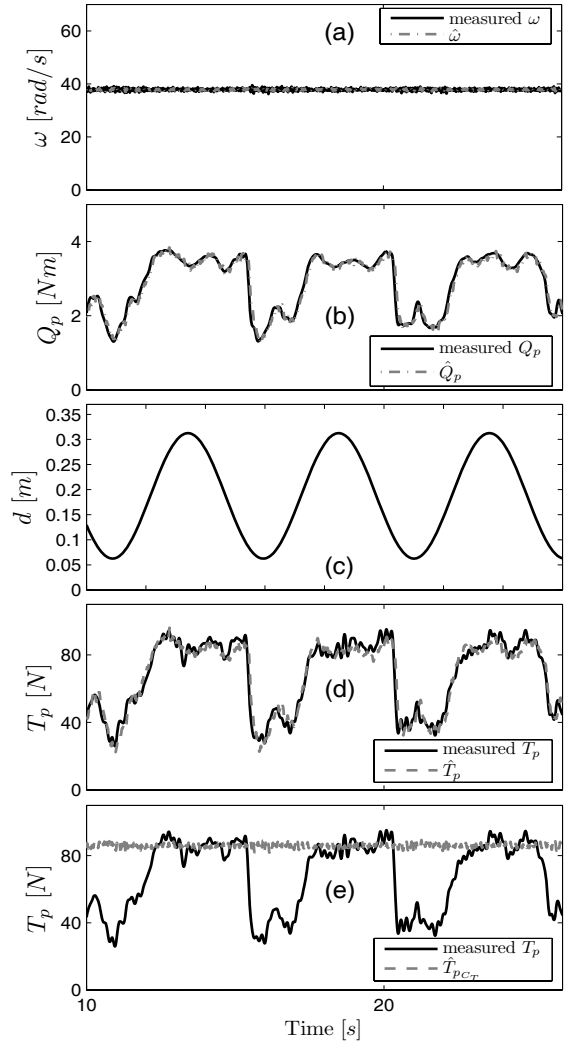


Fig. 18. Data from the experiment with waves.

$$P_1 = \begin{bmatrix} p_{11} & p_{12} \\ p_{12} & p_{22} \end{bmatrix}, \tag{29}$$

we can compute its time derivative along the trajectory of (19) obtaining

$$\begin{aligned} \dot{V} = \quad & -\left[\tfrac{1}{J_m} p_{11}\left(k_{f_2}+l_1\right) - p_{12} l_2\right] \tilde{e}_1^2 - \left[\tfrac{p_{22}}{\tau_1} + \tfrac{p_{12}}{J_m}\right] \tilde{e}_2^2 \\ & - \left[\tfrac{p_{12}}{J_m}\left(k_{f_2}+l_1\right) + \tfrac{p_{12}}{\tau_1} + \tfrac{p_{11}}{J_m} - p_{22} l_2\right] \tilde{e}_1 \tilde{e}_2 \\ & - p_{12}\psi(\tilde{e}_1,\hat{\omega})\tilde{e}_2 - p_{11}\psi(\tilde{e}_1,\hat{\omega})\tilde{e}_1. \end{aligned} \tag{30}$$

From the nonlinearity $\psi(\tilde{e}_1,\hat{\omega})$ we can subtract the linear function $\alpha\tilde{e}_1$, where $\alpha$ is constant and satisfies A1, such that

$$g_1(\tilde{e}_1,\hat{\omega}) = \psi(\tilde{e}_1,\hat{\omega}) - \alpha\tilde{e}_1. \tag{31}$$

Since the graph of $\psi(\tilde{e}_1,\hat{\omega})$ belongs to the sector $[0,\alpha]$, the graph of $g(\tilde{e}_1,\hat{\omega})$ belongs to the sector $[-\alpha,\ \alpha]$, i.e.

$$\forall \tilde{e}_1, \forall \hat{\omega} : \left[g(\tilde{e}_1,\hat{\omega})\right]^2 < \alpha^2 \tilde{e}_1^2. \tag{32}$$

Substituting (31) in (30) and recalling that, since $p_{11} > 0$, $p_{11}\psi(\tilde{e}_1,\hat{\omega})\tilde{e}_1 > 0$ we get

$$\begin{aligned} \dot{V} \leq \quad & -\left[\tfrac{1}{J_m} p_{11}\left(k_{f_2}+l_1\right) - p_{12} l_2\right] \tilde{e}_1^2 - \left[\tfrac{p_{22}}{\tau_1} + \tfrac{p_{12}}{J_m}\right] \tilde{e}_2^2 \\ & - \left[\tfrac{p_{12}}{J_m}\left(k_{f_2}+l_1\right) + \tfrac{p_{12}}{\tau_1} + \tfrac{p_{11}}{J_m} - p_{22} l_2 + p_{12}\alpha\right] \tilde{e}_1 \tilde{e}_2 \\ & - p_{12} g_1(\tilde{e}_1,\hat{\omega})\tilde{e}_2. \end{aligned} \tag{33}$$

Choosing $p_{12} > 0$, we can use Young's inequality

$$-2xy \leq \mu x^2 + \frac{1}{\mu} y^2 \quad \forall \mu > 0,$$

on the last term of (33) obtaining

$$\begin{aligned} -p_{12} g_1(\tilde{e}_1,\hat{\omega})\tilde{e}_2 \quad & \leq \mu \tfrac{p_{12}}{2} \tilde{e}_2^2 + \tfrac{p_{12}}{2\mu} \left[g_1(\tilde{e}_1,\hat{\omega})\right]^2 \\ & \leq \mu \tfrac{p_{12}}{2} \tilde{e}_2^2 + \tfrac{p_{12}}{2\mu} \alpha^2 \tilde{e}_1^2. \end{aligned} \tag{34}$$

Using (34) in (33) we attain

$$\begin{aligned} \dot{V} \leq \quad & -\left[\tfrac{1}{J_m} p_{11}\left(k_{f_2}+l_1\right) - p_{12} l_2 - \tfrac{p_{12}}{2\mu}\alpha^2\right] \tilde{e}_1^2 \\ & - \left[\tfrac{p_{12}}{J_m}\left(k_{f_2}+l_1\right) + \tfrac{p_{12}}{\tau_1} + \tfrac{p_{11}}{J_m} - p_{22} l_2 + p_{12}\alpha\right] \tilde{e}_1 \tilde{e}_2 \\ & - \left[\tfrac{p_{22}}{\tau_1} + \tfrac{p_{12}}{J_m} - \mu\tfrac{p_{12}}{2}\right] \tilde{e}_2^2. \end{aligned} \tag{35}$$

Selecting $l_2 > 0$ and $p_{22}$ such that

$$p_{22} = \frac{1}{l_2}\left[\frac{p_{12}}{J_m}\left(k_{f_2}+l_1\right) + \frac{p_{12}}{\tau_1} + \frac{p_{11}}{J_m} + p_{12}\alpha\right], \tag{36}$$

the cross-term in (35) is cancelled. To obtain a negative definite $\dot{V}$ the following are needed:

$$\frac{1}{J_m} p_{11}\left(k_{f_2}+l_1\right) - p_{12} l_2 - \frac{p_{12}}{2\mu}\alpha^2 > 0, \tag{37}$$

$$\frac{p_{22}}{\tau_1} + p_{12}\left(\frac{1}{J_m} - \frac{\mu}{2}\right) > 0. \tag{38}$$

Choosing $p_{11} = p_{12}\alpha^2\kappa J_m$ with $\kappa > 0$, the inequality (37) is satisfied for

$$l_1 > -k_{f_2} + \frac{l_2}{\alpha^2\kappa} + \frac{1}{2\mu\kappa}. \tag{39}$$

With this choice of $l_1$, we observe from (36) that $p_{22} > 0$ and the inequality (38) certainly holds if

$$\mu < \frac{2}{J_m}. \tag{40}$$

Combining (39) and (36), we get $p_{22} > \frac{p_{11}}{l_2 J_m}$. This yields

$$P_1 > \begin{bmatrix} p_{11} & \frac{p_{11}}{\alpha^2\kappa J_m} \\ \frac{p_{11}}{\alpha^2\kappa J_m} & \frac{p_{11}}{l_2 J_m} \end{bmatrix}. \tag{41}$$

If $l_2 < \alpha^4\kappa^2 J_m$ then $P_1$ is positive definite. Choosing the observer gains according to A4 and A5 of Proposition 1, the derivative of the Lyapunov function candidate is negative definite since

$$\dot{V} \leq \quad -\min\{q_1, q_2\} \left\|\tilde{e}\right\|_2^2, \tag{42}$$

where

$$q_1 = \frac{1}{J_m} p_{11}\left(k_{f_2}+l_1\right) - p_{12} l_2 - \frac{p_{12}}{2\mu}\alpha^2, \tag{43}$$

$$q_2 = \frac{p_{22}}{\tau_1} + p_{12}\left(\frac{1}{J_m} - \frac{\mu}{2}\right). \tag{44}$$

The observer error dynamics, with $u = 0\ \forall t$, is thus globally exponentially stable (GES). When the input $u$ is different from zero for some $t$, the term $2\tilde{e}^T P_1 B_1 u$ must be added to the

derivative of the Lyapunov function in (42):

$$\begin{aligned}\dot{V} &\leq -\min\{q_1,q_2\}\left\|\tilde{e}\right\|_2^2 + 2\tilde{e}^T P_1 B_1 u \\ &\leq -\min\{q_1,q_2\}\left\|\tilde{e}\right\|_2^2 + 2\left\|\tilde{e}^T P_1 B_1 u\right\|_2 \\ &\leq -\min\{q_1,q_2\}\left\|\tilde{e}\right\|_2^2 + 2\left\|\tilde{e}^T\right\|_2 \left\|P_1\right\|_2 \left\|B_1\right\|_2 \left\|u\right\|_2 .\end{aligned} \tag{45}$$

With $0 < \theta < 1$, we obtain

$$\begin{aligned}\dot{V} &\leq -\min\{q_1,q_2\}\left\|\tilde{e}\right\|_2^2 + \left\|P_1\right\|_2 \left\|B_1\right\|_2 \left\|\tilde{e}\right\|_2 \left\|u\right\|_2 \\ &\leq -(1-\theta)\min\{q_1,q_2\}\left\|\tilde{e}\right\|_2^2 - \theta\min\{q_1,q_2\}\left\|\tilde{e}\right\|_2^2 \\ &\quad + \left\|P_1\right\|_2 \left\|B_1\right\|_2 \left\|\tilde{e}\right\|_2 \left\|u\right\|_2 .\end{aligned} \tag{46}$$

For any $\left\|\tilde{e}\right\|_2$ such that

$$\left\|\tilde{e}\right\|_2 \geq \rho(\left\|u\right\|_2), \tag{47}$$

where

$$\rho(\left\|u\right\|_2) = \frac{\left\|P_1\right\|_2 \left\|B_1\right\|_2}{\theta\min\{q_1,q_2\}}\left\|u\right\|_2 \tag{48}$$

is a (linear) class $\mathcal{K}$ function, we obtain

$$\dot{V} \leq -(1-\theta)\min\{q_1,q_2\}\left\|\tilde{e}\right\|_2^2 \leq 0. \tag{49}$$

Since $V$ is positive definite and radially unbounded, from Theorem 4.19 in [15], the system (19) is ISS. Furthermore, the observer error is uniformly ultimately bounded (UUB) by $\rho\left(\sup_{t>t_0}\left(\left\|u\right\|_2\right)\right)$.

## REFERENCES


[1] R. Bachmayer, L. L. Whitcomb, and M. A. Grosenbaugh, "An accurate four-quadrant nonlinear dynamical model for marine thrusters: Theory and experimental validation," *IEEE Journal of Oceanic Engineering*, vol. 25, no. 1, pp. 146–159, January 2000.

[2] M. Blanke, "Ship propulsion losses related to automatic steering and prime mover control." Ph.D. dissertation, Technical University of Denmark, 1981.

[3] M. Blanke, R. Izadi-Zamanabadi, and T. F. Lootsma, "Fault monitoring and reconfigurable control for ships propulsion plant," *Journal of Adaptive Control and Signal Processing*, vol. 12, pp. 671–688, 1998.

[4] M. Blanke, K. Lindegaard, and T. I. Fossen, "Dynamic model for thrust generation of marine propellers," in *5th IFAC Conference of Manoeuvring and Control of Marine craft (MCMC)*, Aalborg, Denmark, 2000, pp. 363–368.

[5] J. P. Breslin and P. Andersen, *Hydrodynamics of Ship Propellers*. Cambridge University Press, 1994.

[6] J. S. Carlton, *Marine Propellers and Propulsion*. Oxford, U.K.: Butterworth-Heinemann Ltd., 1994.

[7] T. I. Fossen, *Marine Control Systems - Guidance, Navigation, and Control of Ships, Rigs and Underwater Vehicles*. Marine Cybernetics, Trondheim, Norway, 2002.

[8] T. I. Fossen and M. Blanke, "Nonlinear output feedback control of underwater vehicle propellers using feedback from estimated axial flow velocity," *IEEE Journal of Oceanic Engineering*, vol. 25, no. 2, pp. 241–255, April 2000.

[9] P. Gill, W. Murray, and M. Wright, *Practical Optimization*. London, Academic Press, 1981.

[10] C. Guibert, E. Foulon, N. Aït-Ahmed, and L. Loron, "Thrust control of electric marine thrusters," in *31nd Annual Conference of IEEE Industrial Electronics Society. IECON 2005*, Raleigh, North Carolina, USA, 6-10 November 2005.

[11] A. J. Healey, S. M. Rock, S. Cody, D. Miles, and J. P. Brown, "Toward an improved understanding of thruster dynamics for underwater vehicles," *Symp. Autonomous Underwater Vehicle Technology, Boston MA*, pp. 340–352, 1994.

[12] ——, "Toward an improved understanding of thruster dynamics for underwater vehicles," *IEEE Journal of Oceanic Engineering*, vol. 20, no. 4, pp. 354–61, October 1995.

[13] ITTC, *Recommended Procedures - Performance, Propulsion 1978 ITTC Performance Prediction Method - 7.5-02-03-01.4*, International Towing Tank Conference, 1999.

[14] ——, *Recommended Procedures - Testing and Extrapolation Methods. Propulsion, Propulsor, Open Water Test*, International Towing Tank Conference, 2002.

[15] H. K. Khalil, *Nonlinear Systems*, 3rd ed. Prentice Hall, 2000.

[16] J. Kim and W. K. Chung, "Accurate and practical thruster modeling for underwater vehicles," *IEEE Journal of Ocean Engineering*, vol. 33, no. 5-6, pp. 566–586, April 2006.

[17] E. V. Lewis, *Principles of Naval Architecture Vol II: Resistance, Propulsion and Vibration*, 3rd ed. New York: Society of Naval Architects and Marine Engineers, 1988.

[18] T. F. Lootsma, "Observer-based faut detection and isolation for nonlinear systems," Ph.D. dissertation, Aalborg University, Denmark, 2001.

[19] J. Martínez-Calle, L. Balbona-Calvo, J. González-Pérez, and E. Blanco-Marigorta, "An open water numerical model for a marine propeller: A comparison with experimental data," in *ASME FEDSM Joint US-European Fluids Engineering Summer Conference*, Montreal, Canada, 2002.

[20] L. Pivano, T. I. Fossen, and T. A. Johansen, "Nonlinear model identification of a marine propeller over four-quadrant operations," in *14th IFAC Symposium on System Identification, SYSID*, Newcastle, Australia, 2006.

[21] L. Pivano, T. A. Johansen, Ø. N. Smogeli, and T. I. Fossen, "Nonlinear Thrust Controller for Marine Propellers in Four-Quadrant Operations," in *26th American Control Conference (ACC07)*, New York, USA, July 2007.

[22] L. Pivano, Ø. N. Smogeli, T. A. Johansen, and T. I. Fossen, "Experimental Validation of a Marine Propeller Thrust Estimation Scheme," in *7th IFAC Conference on Manoeuvring and Control of Marine Craft (MCMC)*, Lisbon, Portugal, September 2006.

[23] ——, "Marine propeller thrust estimation in four-quadrant operations," in *45th IEEE Conference on Decision and Control*, San Diego, CA, USA, 13-15 December 2006.

[24] D. A. Smallwood and L. L. Whitcomb, "Model Based Dynamic Positioning of Underwater Robotic Vehicles: Theory and Experiment," *IEEE Journal of Oceanic Engineering*, vol. 29, no. 1, pp. 169–186, January 2004.

[25] Ø. N. Smogeli, "Control of Marine Propellers: From Normal to Extreme Conditions," Ph.D. dissertation, Department of Marine Technology, Norwegian University of Science and Technology (NTNU), Trondheim, Norway, September 2006.

[26] Ø. N. Smogeli, J. Hansen, A. J. Sørensen, and T. A. Johansen, "Anti-spin control for marine propulsion systems," in *43rd IEEE Conference on Decision and Control*, Paradise Island, Bahamas, 14-17 December 2004.

[27] Ø. N. Smogeli, E. Ruth, and A. J. Sorensen, "Experimental validation of power and torque thruster control," in *IEEE 13th Mediterranean Conference on Control and Automation (MED'05)*, Cyprus, June 2005, pp. 1506– 1511.

[28] Ø. N. Smogeli, A. J. Sørensen, and T. I. Fossen, "Design of a hybrid power/torque thruster controller with loss estimation," in *IFAC Conference on Control Applications in Marine Systems (CAMS'04)*, Ancona, Italy, 2004.

[29] Ø. N. Smogeli, A. J. Sørensen, and K. J. Minsaas, "The Concept of Anti-Spin Thruster Control," *To appear in Control Engineering Practice (CEP)*, 2007.

[30] M. Vysohlid and K. Mahesh, "Large-eddy simulation of propeller crashback," in *57th Annual Meeting of the Division of Fluid Dynamics*, Seattle, Washington, 21-23 November 2004.

[31] L. L. Whitcomb and D. Yoerger, "Developement, comparison, and preliminary experimental validation of nonlinear dynamic thruster models," *IEEE Journal of Oceanic Engineering*, vol. 24, no. 4, pp. 481–494, Oct. 1999.

[32] D. R. Yoerger, J. G. Cooke, and J. E. Slotine, "The influence of thruster dynamics on underwater vehicle behavior and their incorporation into control system design," *IEEE Journal of Oceanic Engineering*, vol. 15, no. 3, pp. 167–178, June 1990.

[33] V. B. Zhinkin, "Determination of the screw propeller thrust when the torque or shaft power is known," in *Fourth international symposium on practical design of ships and mobile units*, Bulgaria, 23-38 October 1989.